scientific reports

Check for updates

OPEN

Multi-omics analysis of bariatric surgery's impact on type 2 diabetes and prediabetes

Balqees Almazrouei[1,2], Mira Mousa[1,3], Andre Barreiros[1], Nour Al Dain Marzouka[1], Michael Olbrich[1], Sanjay Ramachandran[1], Sreejisha P. Sreedharan[1], Sarah K. Azzam[1], Sarah El Hajj Chehadeh[1], John Rodriguez[4], Juan P. Pantoja[4], Javed Raza[4], Gabriel Diaz Del Gobbo[4], Mohammed Abdallah[4], Juan S. Barajas-Gamboa[4], Syed Salman Ashraf[1,6], Carlos Abril[4], Mohammad Al Bataineh[1,5] & Habiba Al Safar[1,2]✉

Bariatric surgery is a promising intervention for managing obesity-related metabolic disorders; however, its effects on cardiovascular disease (CVD) in individuals with type 2 diabetes (T2D) remain poorly understood. To address this gap, we utilized a multi-omics approach to investigate how bariatric surgery influences Emirati individuals with T2D and prediabetes, focusing on the early detection of CVD markers. We longitudinally profiled 19 patients over a 9-month period, collecting omics data, including whole-genome sequencing (WGS), protein immunoassays, untargeted metabolomics, and 16S rRNA sequencing to determine gut microbiome composition. Through this study, we showed that bariatric surgery reduced CVD risk and inflammatory biomarkers while inducing changes in the gut microbiome and metabolomic profiles. We identified four inflammatory biomarkers (FGF-basic, TNFSF13, IL-8, and IL-1Ra) that were significantly altered following surgery ($p < 0.05$). Additionally, we identified 98 metabolites that showed significant changes after surgery that are involved in folate biosynthesis, glycerophospholipid, and retinol metabolism. Eighteen microbial genera were found to differentiate between the pre- and post-surgery states. Our analysis revealed four microbial genera (*Enterobacter*, *Enterococcus*, *Gemella*, and *Erysipelotrichaceae UCG-003*) associated with two T2D SNPs (rs11830243 and rs6978118) and three CVD SNPs (rs9490306, 62207434, and rs34606058). These genera formed the network's central hub, connecting host genetic variants, metabolic pathways, and clinical data, highlighting their role in host-microbiome interactions. The study quantifies the impact of phenotypic factors on CVD progression among UAE nationals, contributing to a deeper understanding of cardiometabolic health within this population.

Keywords Type 2 diabetes, Bariatric surgery, Omics, Cardiovascular disease, Precision medicine, Risk predictor, Prognosis

Diabetes Mellitus is a chronic metabolic disorder characterized by elevated blood glucose levels due to absolute or relative insulin deficiency[1]. The condition includes several subtypes, such as Type 1 diabetes, Type 2 diabetes, gestational diabetes, and rarer forms linked to genetic or secondary causes. T2D is the most predominant form, with an increasing prevalence in adults and children[2]. The International Diabetes Federation (IDF) estimates that 537 million adults (aged 20–79 years) have been living with diabetes in 2021, a figure projected to reach 643 million by 2030[1]. In the UAE, the age-adjusted prevalence of T2D among individuals aged 20–79 years was estimated at 16.4% by the IDF in 2021[3]. Over the past decades, bariatric surgery has evolved into the most effective treatment for obesity and associated metabolic disorders. Beyond its well-documented role in weight loss, bariatric surgery is recognized as a powerful intervention for glycemic control in patients with T2D[4].

[1]Center for Biotechnology, Khalifa University of Science and Technology, Abu Dhabi, United Arab Emirates. [2]Department of Biomedical Engineering, Khalifa University of Science and Technology, Abu Dhabi, United Arab Emirates. [3]Department of Public Health and Epidemiology, Khalifa University of Science and Technology, Abu Dhabi, United Arab Emirates. [4]Department of General Surgery, Digestive Disease Institute, Cleveland Clinic Abu Dhabi, Abu Dhabi, United Arab Emirates. [5]Department of Basic Medical Sciences, College of Medicine, Yarmouk University, Irbid, Jordan. [6]Department of Biological Sciences, College of Medicine and Health Sciences, Khalifa University of Science and Technology, Abu Dhabi, United Arab Emirates. ✉email: habiba.alsafar@ku.ac.ae

Comprehensive molecular profiling using omics technologies, including genomics, proteomics, metabolomics, and microbiome analysis, plays a crucial role in precision medicine, providing an essential approach to understanding the intricate molecular mechanisms underlying various diseases. It has been employed to identify factors linked to the progression of T2D and its associated conditions[5–7]. Recently, these technologies have been applied to explore the primary outcomes of bariatric surgery, investigate T2D biomarkers, and pave the way for novel treatment strategies for T2D. This approach aids in identifying which patients are most likely to benefit from various therapeutic interventions, including bariatric surgery. While individual studies have explored genetic, proteomic, metabolomic, or microbiome changes independently, only a few have attempted partial integration. For instance, Almby K. et al.[8] examined transcriptomics and proteomics; Härm A. et al.[9] and Zhao S. et al.[10] focused on metabolomics and proteomics; Lau E. et al.[11] investigated the gut microbiome alongside proteomics; Benton M. et al. [12] analyzed epigenomics and transcriptomics; and Vohl M-C et al. [13] integrated epigenomics, transcriptomics, and proteomics. This highlights a critical gap in the literature, underscoring the need for a comprehensive multi-omics approach to fully elucidate the molecular mechanisms underlying the metabolic effects of bariatric surgery in T2D.

Therefore, the aim of this study was to investigate the impact of bariatric surgery on metabolic health, focusing on early signs of CVD, using a multi-omics approach in a cohort of patients with T2D and prediabetes in the UAE. Over a nine-month period, we prospectively collected longitudinal samples and conducted genomics analysis using whole-genome sequencing (WGS), proteomic analysis via protein immunoassays, untargeted metabolomics, and gut microbiome profiling using 16S rRNA sequencing. We developed a correlation network that revealed distinct clusters of interrelated analytes linked to physiological processes and disease progression by integrating the respective datasets. To the best of our knowledge, this study is the first to leverage a multi-omics framework to uncover the molecular mechanisms underlying metabolic improvements in T2D and prediabetes following bariatric surgery, and the first of its kind to be conducted in the Emirati population.

Methods

Ethics statement

Ethical approvals were obtained from the Department of Health – Abu Dhabi (DOH/ADHRTC/2024/1519), the Research Ethics Committee of Khalifa University of Science and Technology (H21-039), and the Cleveland Clinic Abu Dhabi Research Ethics Committee (A-2021-070). Written informed consents were obtained from all individuals after clearly explaining the study participation, which includes a follow-up period of up to nine months before any study procedures occur. The study was performed according to relevant research guidelines and committee regulations.

Study design and population

A total of 19 UAE national patients, aged between 25 and 53 years, including six diagnosed with T2D and thirteen with prediabetes, were recruited from Cleveland Clinic Abu Dhabi to undergo bariatric surgery. Of these, nine received Laparoscopic Sleeve Gastrectomy (SG), five underwent Roux-en-Y Gastric Bypass (RYGB), four underwent Laparoscopic Gastric Bypass (GB), and one underwent Single Anastomosis Duodeno-Ileal Bypass with sleeve gastrectomy (SADI). Samples, clinical and demographic characteristics were collected from recruited patients at baseline (pre-surgery) and at 3-, 6-, and 9-months post-surgery (Supplementary Fig. S1). The inclusion criteria were UAE nationals (holder of a passport and family book), aged 18 to 70 years, diagnosed with T2D or prediabetes according to the American Diabetes Association criteria (T2D: Fasting Plasma Glucose (FPG) ≥ 126 mg/dL or HbA1c ≥ 6.5%; Prediabetes: FPG 100–125 mg/dL or HbA1c 5.7%–6.4%), with a family history of obesity. Participants were required to have undergone primary bariatric surgery, a BMI ≥ 30 kg/m^2 with at least one obesity-related comorbidity, and the ability to undergo regular blood sampling every 3 months over a 9-month period. Individuals with hypertension are defined as having systolic blood pressure ≥ 140 mmHg, diastolic blood pressure ≥ 90 mmHg, or taking medications for high blood pressure.

DNA extraction

Genomic DNA was isolated from whole blood using the QIAamp DNA Blood Mini Kit (Qiagen; Germany) according to the manufacturer's protocol. Microbial DNA was extracted from fecal samples using the QIAamp PowerFecal Pro DNA Kit (Qiagen) following the manufacturer's instructions.

Whole-genome sequencing

DNA libraries were prepared using Illumina's DNA PCR-Free library kit (Illumina; USA). Libraries were quantified using the KAPA Library Quantification Kit (Roche; USA) on the ViiA 7 Real-Time PCR System. The WGS libraries were pooled and subsequently sequenced using Illumina's NovaSeq 6000 system, targeting a minimum mean depth of 25X. Raw sequencing reads were demultiplexed, and the Binary Base Call (BCL) files generated by the Illumina sequencing system were converted to FASTQ format using the bcl2fastq tool (Illumina). Reads were then aligned to the human reference genome (GRCh38), and variant calling was performed using Sentieon v.202308.03 (California, USA; https://www.sentieon.com/).

Protein immunoassay

Plasma inflammatory markers were quantified using the Bio-Plex Pro™ Human Inflammation Panel 1 (37-plex) and Bio-Plex Pro™ Human Cytokine Panel 1 (27-plex) (Bio-Rad; USA) on the BioPlex-200 system (Bio-Rad). Additionally, serum concentrations of Myoglobin (Beckman Coulter), High-Sensitivity Troponin I (hsTnI) (Beckman Coulter), and B-type natriuretic peptide (BNP) (Beckman Coulter) were analyzed using the Access 2 Immunoassay Analyzer (Beckman Coulter), following the manufacturer's guidelines.

Untargeted metabolomics profiling

Metabolomic profiling was carried out using a qualitative Quadrupole Time-of-Flight liquid chromatography-tandem mass spectrometry technique (LC-MS/MS; X500R Q-TOF; SCIEX; USA). Plasma samples were prepared using protein precipitation method with ice-cold methanol (1:4 v/v). The supernatant was filtered using a 0.22 µm Cellulose Acetate filter and transferred to HPLC amber autosampler vials. A volume of 20 µl of samples was injected into the chromatographic system. Each sample was analyzed in two analytical replicates, and two technical replicates were injected from the same sample. Six blank samples consisting of the mobile phase (A: UPLC/MS grade water (CARLO ERBA; Italy) and 0.1% formic acid (CARLO ERBA), and B: LC/MS Acetonitrile (CARLO ERBA) and 0.1% formic acid, A:B (9:1 v/v)) were analyzed in duplicates. To ensure the reproducibility of retention times and assess data quality, quality control samples were prepared by pooling 10 µl from each sample and analyzed every eighth injection. Additionally, the system was calibrated after every five samples. The separation was done using Kinetex 2.6 µm F5 Column 150 × 2.1 mm (Phenomenex) for both negative and positive models. The injection volume was 20 µl, and the column temperature was 40 °C. The mobile phase consisted of (A) UPLC/MS grade water (CARLO ERBA) and 0.1% formic acid (CARLO ERBA), and (B) LC/MS Acetonitrile (CARLO ERBA) and 0.1% formic acid. The elution program of the pump gradient was set as follows: t = 0 min, 2% B; t = 2, 2% B; t = 3, 5% B; t = 5, 80% B; t = 13, 95% B; t = 16.5, 95% B; t = 17, 2% B; t = 20, 2% B. The flow rate was set to 0.3 mL/min, and the injection needle was washed after each sample for 5 s with 25:25:25:25; water/isopropyl alcohol/methanol/acetonitrile. Turbolon Spray was used as an ion source for positive and negative modes with a voltage of 5.5 kV. The collision energy was set at 35 V, and the declustering potential was set at 60 V. To obtain a richer MS/MS spectrum, the collision energy spread was set at 15 V. The intervals of the mass scan were 50–1000 Da for both MS and MS/MS.

Microbial profiling using 16S rRNA sequencing

Isolated microbial DNA was PCR-amplified with 16S Amplicon PCR forward and reverse primers (Integrated DNA Technologies) targeting the V3-V4 region using 2 × KAPA HiFi HotStart ReadyMix (Roche). The primer sequences were as follows: 16S Amplicon PCR forward primer: *5'-TCGTCGGCAGCGTCAGATGTGTATAAGAGACAGCCTACGGGNGGCWGCAG-3'* and the 16S Amplicon PCR reverse primer: *5'*-GTCTCGTGGGCTCGGAGATGTGTATAA *GAGACAGGACTACHVGGGTATCTAATCC-3'*. The index PCR step was implemented to attach dual indices and Illumina sequencing adapters using the Nextera XT Index Kit v2 Set A (Illumina). The libraries were run on the Illumina MiSeq system using the MiSeq Reagent Kit v3 (600 cycles) (Illumina).

Statistical analysis

Age differences were analyzed using a one-way ANOVA test and the comparison of sex distributions was performed using the Chi-squared test. For follow-up comparisons, the *p*-value was calculated using a paired t-test with a two-tailed approach.

Variants from WGS data were filtered, prioritized, and classified using Franklin (Genoox; https://franklin.genoox.com/) as the primary analysis platform, following the American College of Medical Genetics and Genomics (ACMG) criteria. The initial filtering retained variants with sequencing depth ≥ 11 while excluding those that failed Franklin's confidence score assessment. Manual verification of variants and their population frequencies was performed using the VarSome human genomic variant search engine (v12.9.0; https://varsome.com)[14], which incorporates data from the Genome Aggregation Database (gnomAD v4.1). Variants located within segmental duplication regions were flagged to highlight the potential for false positives.

Statistical analyses of protein immunoassay mean values were performed using GraphPad Prism 10 (https://www.graphpad.com/). Concentrations marked as "< OOR" (out of range) were imputed by replacing them with half the minimum concentration detected for the respective protein. The data distribution was assessed for normality using the Shapiro–Wilk and Kolmogorov–Smirnov tests. Continuous data points were analyzed using one-way ANOVA with the Bonferroni post-hoc test. Differences with p-values ≤ 0.05 were considered statistically significant. Results are reported as mean concentrations (pg/mL) ± the standard error of the mean (SEM).

Metabolomics data were compiled into a compound library with the NIST 2017 database in LibraryView™ software (v.1.6, SCIEX; https://sciex.com/). The acquired data was pre-processed using R and the MetaboAnalyst platform (v.6.0, https://www.metaboanalyst.ca/)[15]. A list of m/z features with their intensities was generated. Peak identification was performed using Sciex OS (SCIEX) software from the area under the curve. Metabolite identification was performed by accurately matching library hit ≥ 70 and mass error (ppm) of -5 to 5. The standard *DESeq2* pipeline version 3.20[16] was used to find the most significant difference in the fold change between the metabolites of pre- and post-surgery. The analysis design was corrected for patients with multiple samples post-surgery using the equation design = ~Patient_id + surgery. The principal component analysis (PCA) was computed using the *FactoMineR* R package[17], and the *factoextra* R package[18] was used to extract and visualize the results. Metabo-Analyst[15] and WebGestalt (2024; https://www.webgestalt.org/)[19] were used for pathway enrichment analysis.

FASTQ files of paired-end sequencing reads of the 16 s rRNA were analyzed using the DADA2 R package in Rstudio (v.3.4.1)[20]. Taxonomy assignment was done using the naive Bayesian classifier method using the SILVA 16S rRNA database (v.138.1) *silva_nr99_v138.1_train_set.fa.gz*, and species were assigned with the *silva_species_assignment_v138.1.fa.gz* library. At the final stage of the pipeline, the amplicon sequence variants (ASVs) were compiled into a *Phyloseq* object for downstream analysis[21]. The Wilcoxon test determined significant differences in Alpha diversity indices utilizing Chao1, Shannon, and Simpson indices. The beta diversity was assessed by Permutational analysis of variance (PERMANOVA) on Bray–Curtis dissimilarities using the *adonis* function from the *vegan* package in R. The differential abundance analysis followed the standard DESeq2 pipeline with

a prefilter where the bacterial genus had more than 10 counts in at least 20% of samples. A bacterial genus is considered significant if its False Discovery Rate (FDR) q-value is < 0.05 and abs (Log_2(FC)) > 0.1. The analysis design was corrected for patients with multiple samples post-surgery by using the equation design = ~ Patient_id + Surgery. Functional profiling of microbial communities was conducted using the Phylogenetic Investigation of Communities by Reconstruction of Unobserved States (PICRUSt2) prediction algorithm and functional analysis used the standard *DESeq2* workflow version 3.20[16]. The differentially abundant metabolic pathways were annotated based on the MetaCyc database.

To normalize data for association analysis, the ratios of pre-surgery to average post-surgery values (post + 1) were calculated to assess changes over time while accounting for variability in sample availability across time points. The resulting ratios were then log_2-transformed to enable appropriate statistical comparisons across omics layers and individuals in the study cohort. Association analysis was performed using the *Matrix_eQTL_engine* R package (v2.1.0)[22], applying a linear regression model via the *modelLinear* function to map Quantitative Trait Loci (QTLs) while adjusting for age and sex as covariates. The analysis was focused on identifying associations between the SNPs of interest (*i.e.,* related to T2D and CVD) and the different molecular data types (protein levels, metabolites, and genera abundance). Only SNPs found in at least three patients (18%) were retained for further analysis. All statistical analyses were carried out using R, with a significance threshold set at FDR < 0.05 for all associations. FDR was computed using the Benjamini–Hochberg method[23], and log (Odds ratio) was used to obtain the effect size (β), where a positive β indicates a direct (positive) association, and a negative β indicates an inverse (negative) association. Clinical variables with > 20% missing data were excluded from downstream analysis. Missing clinical data (< 20%) were imputed using predictive mean matching via the Multivariate Imputation by Chained Equations (*mice*) R package[24]. The differential analysis was conducted separately for each layer using the *voom-limma* package[25]. Within each layer, features were normalized using a centered log-ratio (CLR) transformation to account for compositionality. Pairwise correlations between features from different omics layers were assessed using Spearman's correlation, and FDR-adjusted q-values were calculated for multiple testing corrections. This process was repeated across all pairwise comparisons of the omics layers. Significant correlations (q-value < 0.05) were used to construct a network, where nodes represented the omics features and edges indicated significant correlations between them. The resulting list of nodes and edges was visualized using the igraph v2.1.4 software (https://igraph.org/)[26]. The chord plot was generated using the *chordDiagram* method in the *circlize* R package version 0.4.16[27].

Results

The outcomes of bariatric surgery: clinical measurements, proteomics and metabolomics measures

The clinical and demographic characteristics of the patients at baseline (pre-surgery) and at 3, 6, and 9 months post-bariatric surgery were presented in Table 1 and Fig. 1a–d. After comparing 9 months post-surgery to pre-surgery levels, all patients exhibited significant reductions in fasting glucose ($p = 0.0466$) and HbA1c levels ($p = 0.0464$) over time. Additionally, lipid profile analysis revealed a significant reduction in triglyceride levels ($p = 0.0382$). The blood pressure data indicate a significant improvement in both systolic ($p = 0.0014$) and diastolic ($p = 0.0022$) blood pressure at 9 months post-surgery. Concerning the BMI, it steadily declined over time ($p < 0.0001$) resulting in the reclassification of participants from the "morbidly obese" to the "overweight" category (Fig. 1d). Sex differences in weight loss patterns were also evident, with females achieving higher Excess Body Weight Loss (EBWL) at 9 months, while males demonstrated greater EBWL at 3 months and maintained consistent reductions throughout follow-ups (Fig. 1b).

The impact of bariatric surgery on more than 30 key inflammatory and cardiovascular regulatory proteins was evaluated in Supplementary Figs. S2 and S3. Protein immunoassay identified significant alterations in circulating proteins associated with inflammation. Notably, four key inflammatory biomarkers FGF-basic, TNFSF13, IL-8, and IL-1Ra exhibited significant changes after bariatric surgery ($p < 0.05$) (Fig. 1e).

In addition, an untargeted metabolomics profiling was performed to characterize metabolomic changes pre- and post-bariatric surgery, identifying 745 and 226 metabolites in positive and negative ionization modes, respectively. The analysis focused on overrepresented subsets, highlighting the top 100 differentially abundant metabolites for clearer interpretability. Each individual's metabolic profile was observed to be distinct, with a very low number of metabolites consistently altered across all participants following the surgery. Interestingly, no patient's three post-surgery time points (3, 6, and 9 months) clustered together, indicating substantial variability in metabolic profiles over time. This further supported the decision to average post-surgery data for a more robust comparison between pre- and post-surgery metabolic states. By aggregating the post-surgery data, we aimed to increase statistical power and provide a more comprehensive representation of the overall metabolic changes following bariatric surgery. Fold change analysis identified 98 significantly different metabolites as distinguishing features between pre- and post-surgery groups (Fig. 2a and Supplementary Fig. S4). These metabolites are enriched in folate biosynthesis ($p = 0.0821$), glycerophospholipid metabolism ($p = 0.00477$), and retinol metabolism ($p = 0.0523$) (Fig. 2b).

Taxonomic analysis reveals significant differences in gut microbiome beta diversity at the genus level before and after bariatric surgery

The gut microbiome was analyzed to assess the microbial diversity, relative abundance, and functional composition. *Firmicutes* were the dominant phylum in both pre- and post-surgery samples, but individual responses varied noticeably, with a slight reduction in their relative proportion after surgery. *Bacteroidota* was the second most abundant phylum, showing a slight increase in some post-surgery patients. To investigate features of dysbiosis at the phylum level, specifically imbalances in microbial richness and functional capacity, we examined the Firmicutes-to-Bacteroidetes (F/B) ratio. Pre-surgery patients exhibited an elevated F/B ratio,

	Pre–surgery	3–months post–surgery	6–months post–surgery	9–months post–surgery	*p*–value (9–months vs. baseline)
Demographic parameters					
Age (years)	35.6 ± 8.87	–	–	–	0.887†
Male/Female	9.0/10 (47%/53%)	–	–	–	0.934‡
Weight (kg)	118.8 ± 19.45	98.34 ± 11.66	90.15 ± 13.77	87.6 ± 13.09	***p* < 0.0001***
BMI (kg/m^2)	42.27 ± 5.57	34.42 ± 2.36	31.97 ± 2.354	30.91 ± 2.42	***p* < 0.0001***
EBWL (%)	–	45.57 ± 25.41	62.92 ± 13.01	68.25 ± 13.85	–
TWL (%)	–	16.14 ± 4.88	24.6 ± 5.58	26.51 ± 5.04	–
Blood pressure					
Systolic BP (mmHg)	129.2 ± 14.89	126.2 ± 10.94	123.17 ± 11.99	105 ± 9.839	**0.0014***
Diastolic BP (mmHg)	79.79 ± 9.65	73.8 ± 4.438	75.83 ± 8.75	66.83 ± 9.020	**0.0022***
Lipid profile (mmol/L)					
Total cholesterol	4.91 ± 1.34	4.52 ± 0.765	4.589 ± 0.483	4.71 ± 0.558	0.441
LDL cholesterol	3.30 ± 1.18	2.923 ± 0.8	3.119 ± 0.483	3.105 ± 0.576	0.3598
HDL cholesterol	1.29 ± 0.41	1.304 ± 0.291	1.344 ± 0.360	1.503 ± 0.327	0.2968
Non–HDL cholesterol	3.68 ± 1.35	3.51 ± 0.974	3.243 ± 0.509	3.2 ± 0.648	0.1782
Triglycerides	1.57 ± 1.21	1.176 ± 0.359	0.999 ± 0.312	0.922 ± 0.273	**0.0382***
Biochemistry					
HbA1C (%)	6.23 ± 1.07	5.65 ± 0.838	5.517 ± 0.685	5.388 ± 0.591	**0.0464***
Hemoglobin (g/L)	133.1 ± 13.40	135.3 ± 14.57	129.43 ± 11.18	127.9 ± 15.27	0.2942
Glucose (mmol/L)	6.64 ± 1.88	5.029 ± 0.468	5.025 ± 0.443	4.85 ± 0.45	**0.0466***
Creatinine (µmol/L)	61.53 ± 16.34	60.43 ± 11.12	56.75 ± 7.066	58.25 ± 10.39	0.9314
Ferritin (mcg/L)	109.55 ± 116.269	194.5 ± 0.778	131.3 ± 163.7	109.2 ± 108.6	0.3444
Iron (µmol/L)	10.39 ± 4.16	13.07 ± 4.192	12.91 ± 4.634	16.43 ± 5.087	**0.0058***
Vitamin B12 (pmol/L)	294.69 ± 119.09	603.7 ± 151.7	501.1 ± 178.7	423.6 ± 178.9	0.5658
Vitamin B1 (nmol/L)	102.4 ± 25.05	89.43 ± 21.49	114.4 ± 23.44	115.8 ± 29.27	**0.0852***
Vitamin D (nmol/L)	58.62 ± 31.15	67.8 ± 12.16	56.9 ± 4.384	58.2 ± 10.75	0.8648
Albumin (g/L)	54.95 ± 59.93	41.29 ± 4.309	42.0 ± 2.38	43 ± 2.778	0.3798
Neutrophils (× 10^9/L)	4.69 ± 1.77	3.733 ± 1.381	3.136 ± 1.306	2.963 ± 0.931	**0.0152***
Transferrin (g/L)	2.66 ± 0.357	2.2 ± 0.265	2.50 ± 0.456	2.529 ± 0.475	1.0
TSH (mIU/L)	2.627 ± 2.99	1.575 ± 0.981	1.446 ± 0.616	1.613 ± 0.936	0.5602

Table 1. Clinical and demographic characteristics at baseline and at 3, 6, and 9 months post-bariatric surgery. Data are presented as the mean ± standard deviation (SD) or as counts (n), and age is presented as mean ± SD. *BMI* body mass index, *EBWL* Excess body weight loss, *%TWL* Percent total weight loss, *BP* blood pressure, *LDL* Low-density lipoprotein, *HDL* High-density lipoprotein, *HbA1c* glycosylated hemoglobin, *TSH* thyroid stimulating hormone. *p*-value was calculated using a paired t-test with a two-tailed approach. *$p \leq 0.05$ was considered significant. †: One-way ANOVA test. ‡: Chi-squared test.

indicative of dysbiosis. This ratio significantly decreased following surgery, suggesting a shift toward a healthier and more balanced gut microbiome (Supplementary Fig. S5a,b). At the class level, a reduction in *Clostridia* post-surgery is accompanied by an increase in *Gammaproteobacteria*, *Verrucomicrobiae*, and *Bacilli* (Supplementary Fig. S5c,d). On the other hand, changes in the relative abundance were also observed at the order and family levels (Supplementary Fig. S6). The microbial composition demonstrates a higher prevalence of orders such as *Bacteroidales* and *Lachnospirales* with significant inter-patient variability. Following surgery, the microbial composition underwent significant changes with a notable increase in the relative abundance of orders such as *Acidaminococcales*, *Enterobacterales*, and *Lactobacillales* and a decrease in *Oscillospirales*, *Lachnospirales*, and *Bifidobacteriales* in most patients. Individual variation persists post-surgery in certain orders, such as *Veillonellales-Selenomonadales* and *Verrucomicrobiales*. At the family level, pre-surgery samples are dominated by families such as *Bacteroidaceae* and *Lachnospiraceae*, with significant inter-patient variability. Post-surgery, families like *Acidaminococcaceae*, *Akkermansiaceae*, *Enterobacteriaceae*, and *Streptococcaceae* increased in abundance, while *Bacteroidaceae*, *Lachnospiraceae*, and other less prominent families decreased in most patients.

At the genus level, taxonomy analysis revealed significant changes in each patient's gut microbial composition before and after bariatric surgery (Fig. 3a). Notably, *Bacteroides* exhibited significant variability among patients within the same surgical category, accounting for a substantial proportion of the microbiome in most individuals. However, in cases where *Bacteroides* represented a smaller proportion, genera such as *Dorea* and *Escherichia-Shigella* occupied a larger share of the microbiome. The taxonomical composition of the genera was averaged for pre- and post-surgery patients, as shown in Fig. 3b. An increase in the relative abundance of bacterial genera was identified post-surgery in *Akkermesia*, *Escherichia-Shigella*, and *Streptococcus*, with *Streptococcus* being the only

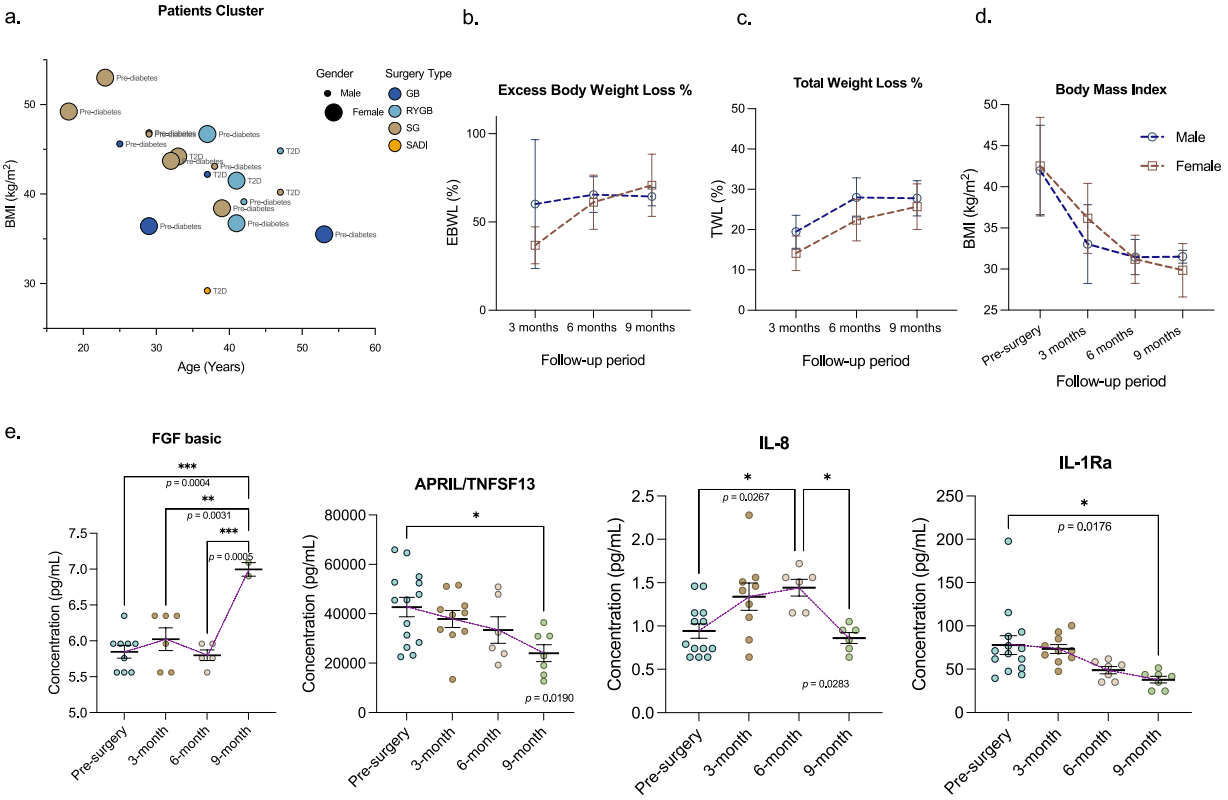

Fig. 1. Patient demographics and changes in inflammatory biomarkers. (**a**) Bubble plot illustrating patients cluster by sex and surgery type based on BMI and age. (**b**, **c**) The percent mean increases in EBWL and TWL after surgery. (**d**) BMI decreases over time after surgery in patients of both genders. (**e**) Significant changes in inflammatory biomarkers measured before surgery and at 3-, 6-, and 9-months post-surgery. Colored dots represent the patients, while the purple dotted line is a visual guide that indicates the transitions between time points. Results were analyzed using a one-way ANOVA with Bonferroni post-hoc test for time differences. Data are expressed as mean ± standard deviation. * $p < 0.05$.

genus consistently enriched across all post-surgery patients. On the other hand, *Agothbacter*, *Bifidobacterium,* and *Faecalibacterium* were significantly reduced in post-surgery groups.

To evaluate the diversity of genera within each patient, the alpha diversity was calculated using three indices: Chao1, Shannon, and Simpson indices (Fig. 3c). While some genera demonstrated differences in relative abundance between pre- and post-surgery samples, the overall alpha diversity metrics indicated no significant difference in genera richness or evenness (Chao1 $p = 0.87$, Shannon $p = 0.97$, and Simpson $p = 0.87$). However, when examined at higher taxonomic levels, including phylum, class, order, and family, alpha diversity showed statistically significant differences between the two time points (Supplementary Fig. S7), suggesting broader structural shifts in the gut microbial community following surgery. In addition, the beta diversity analysis using Bray–Curtis dissimilarity significantly differs between the two groups, as demonstrated by the distinct clustering in the principal coordinates analysis (PCoA) plot in Fig. 3d. The statistically significant change was confirmed using the Multifactorial permutational analysis of variance (PERMANOVA), where the p-value equals 0.0001.

The differential abundance analysis was carried out to determine the statistical differences in the abundances of individual taxa at the genus level between pre- and post-surgery groups. A total of eighteen significant bacterial taxa were identified, evenly split between those enriched in each patient group. The differential abundance analysis of bacterial genera before and after bariatric surgery is shown in Fig. 4a,b. *Streptococcus* was the most significantly enriched bacterial genus in post-surgery patients. It has the smallest FDR q-value $= 2.09 \times 10^{-6}$ and p-value $= 4.22 \times 10^{-6}$. On the other hand, *Agathobacter* is the most significant genus enriched in patients before surgery and the most significant in terms of FDR q-value $= 1.17 \times 10^{-6}$ and p-value $= 1.18 \times 10^{-8}$.

The functional analysis identified a total of 72 metabolic pathways that are significantly distinguished between the pre- and post-surgery groups (Fig. 4c). Most pathways, including antibiotic resistance, biosynthesis, central metabolism, amino acid metabolism, and carbohydrate metabolism, were enriched post-surgery, suggesting increased microbial metabolic activity and adaptive responses to the post-surgical environment. However, the P221-PWY: octane oxidation pathway, which is a member of the hydrocarbon degradation superclass, was enriched pre-surgery. The largest parts of these pathways are the superclass Amino acid metabolism and Biosynthetic pathways.

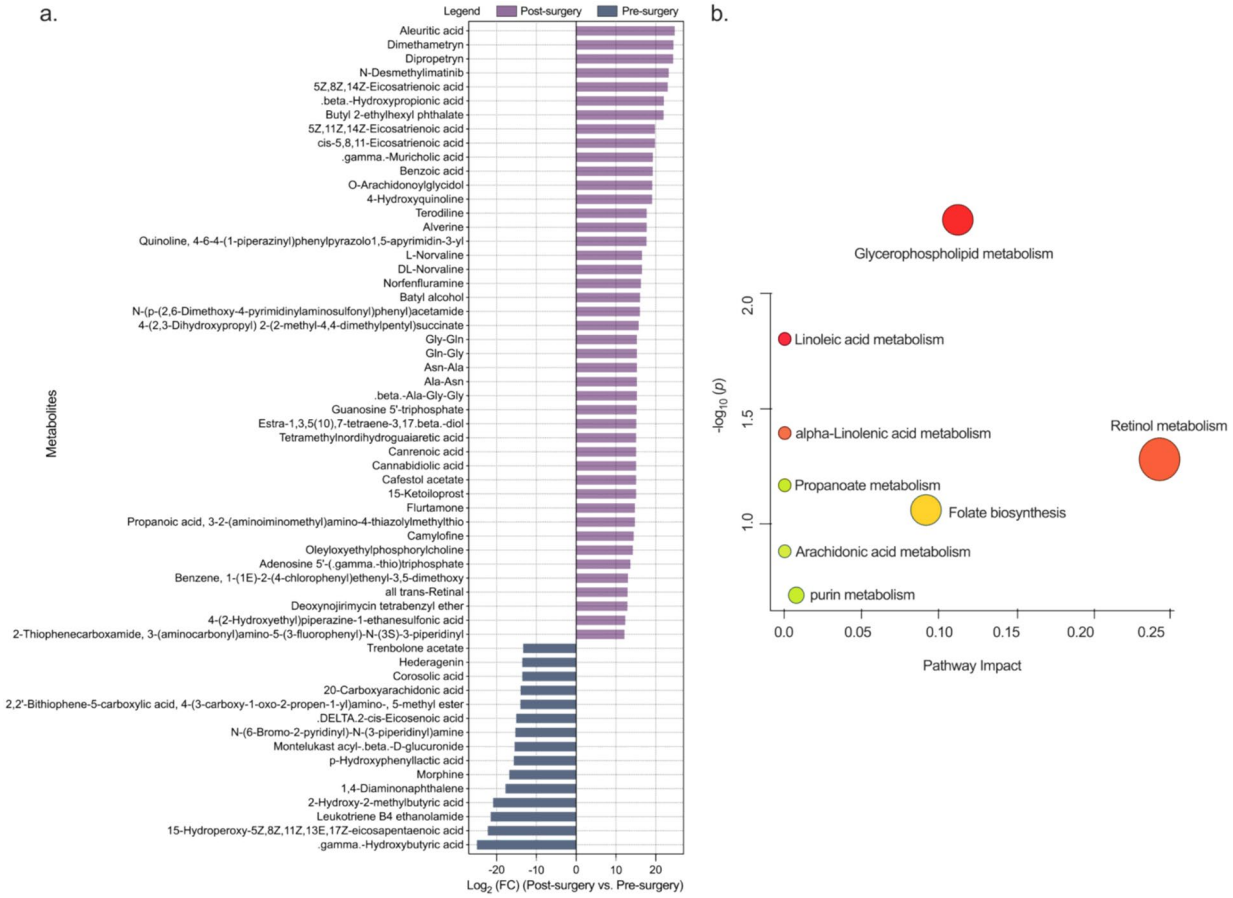

Fig. 2. Enrichment of metabolites and metabolic pathways. (**a**) Bar plot showing the fold changes of differential metabolites before and after bariatric surgery. Each bar represents an individual metabolite, with purple indicating increased pre-surgery levels and blue indicating decreased post-surgery levels. The fold changes were calculated as the ratio of metabolite levels in post-surgery samples to pre-surgery samples and log-transformed (Log_2 FC). The horizontal axis represents the magnitude of change, while the vertical arrangement shows the metabolites sorted by fold change. The complete list is provided in Supplementary Data Fig. S4. (**b**) A bubble diagram illustrating an overview of KEGG[28] metabolic pathway enrichment. Each bubble corresponds to a specific pathway. The statistics of the enriched pathways are summarized in Supplementary Table S1.

Uncovering key associations between genetic variation with inflammatory proteins, metabolites, and microbial genera

A Quantitative Trait Locus (QTL) association analysis investigated the potential host genetic influence on inflammatory proteins, metabolites, and gut microbiome composition (Supplementary Figs. S8, S9). It focused specifically on T2D- and CVD-associated SNPs and their relationship with omics. The T2D and CVD-associated SNPs were selected from the GWAS Catalog based on previously reported associations in published studies up to April 2023. A total of 2,066 T2D-related SNPs and 4,384 CVD-related SNPs were extracted from the WGS data. The analysis aimed to identify proteins, metabolites, and microbiomes that exhibit significant associations with genetic variations in bariatric surgery patients. The association analysis was performed for pre-surgery omics data, and a ratio of (pre)/(average post + 1) was calculated to assess longitudinal changes.

The previously analyzed inflammatory proteins were tested for association with genetic variants; however, none achieved statistical significance of $FDR < 0.05$ (Supplementary Table S2). In the SNPs-metabolites association, ninety significant associations were reported between T2D SNPs and pre-surgery metabolites data. In contrast, 373 significant associations were identified between CVD SNPs and pre-surgery metabolites. *8-Isoprostaglandin-F2-alpha* displayed the strongest positive association with rs115597883 T2D SNP ($\beta = 15.315$, $p = 1.375 \times 10^{-23}$). The same metabolite showed a significant association with the CVD SNP rs12153243 ($\beta = 15.315$, $p = 1.375 \times 10^{-23}$). However, the strongest association of CVD SNPs-metabolites was between rs2312403 and *.gamma.-Muricholic acid* ($\beta = -16.657$, $p = 6.213 \times 10^{-26}$). The longitudinal analysis yielded 1,547 associations between T2D-related SNPs and 845 metabolites, along with 3,291 associations involving CVD-related SNPs, based on data from eight patients. Out of these, 1,341 significant associations (FDR < 0.05) were present between T2D SNPs and metabolites, while 2,894 significant associations were present between CVD SNPs and metabolites. Among the findings, *Heptadecasphing-4-enine-1-phosphate* showed the strongest

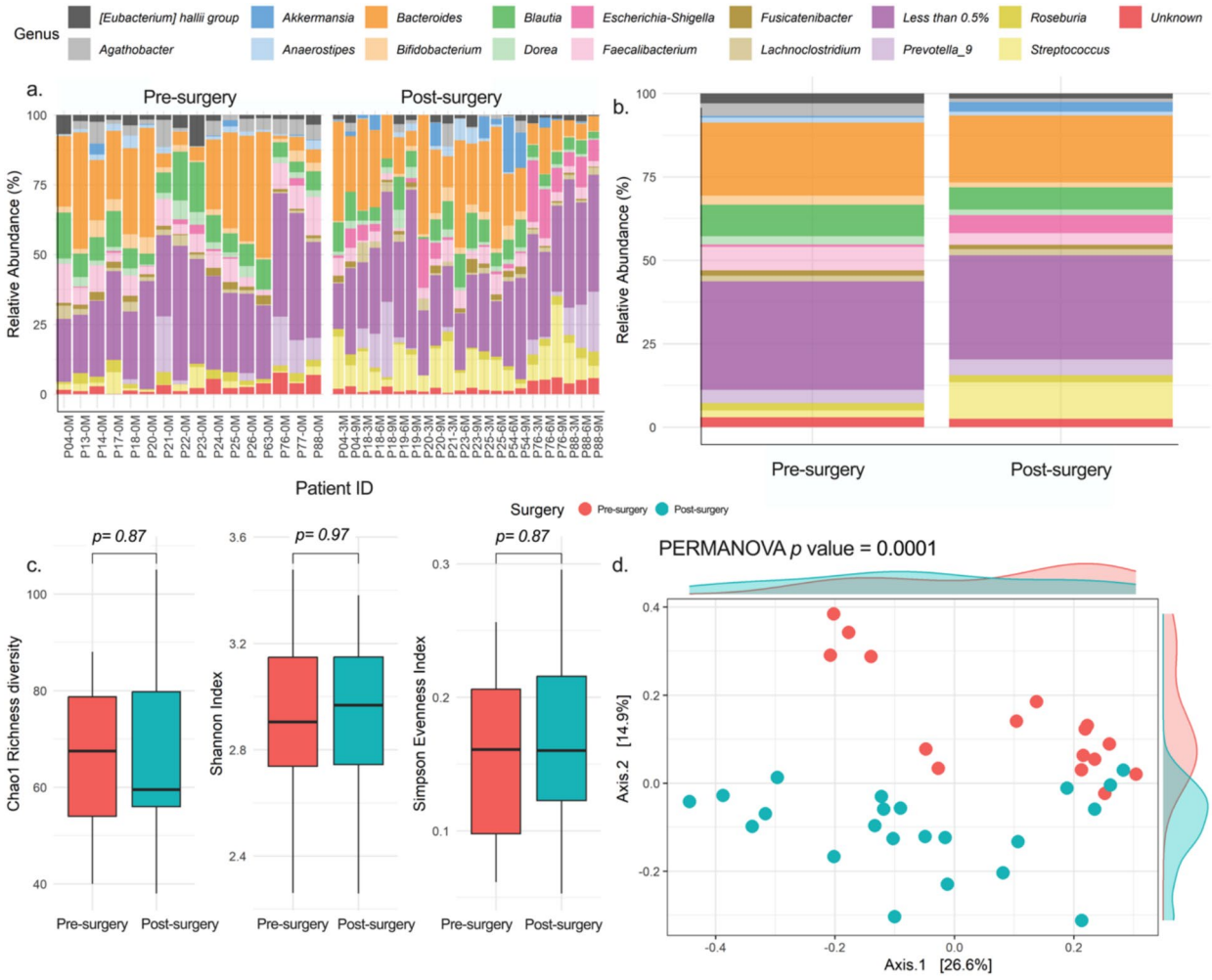

Fig. 3. Microbial composition and diversity analysis between patients' gut microbiome before and after surgery at the genus level. (**a**) The plot shows the relative abundance of the bacterial genus in each patient pre-surgery and 3-, 6-, and 9-months post-surgery. (**b**) The average order level abundance across all patients pre- and post-surgery. (**c**) Alpha diversity plot comparing pre- and post-groups using Chao1, Shannon, and Simpson indices, analyzed using the Wilcoxon test. The overall alpha diversity metrics showed no significant difference in genera richness or evenness (Chao1 $p = 0.87$, Shannon $p = 0.97$ and Simpson $p = 0.87$). (**d**) The beta diversity is presented as a PCoA using the Bray–Curtis (dissimilarity) distance comparing the two groups. The density plots on the axis show the resulting distribution of the samples on each axis. A PERMANOVA test was performed to check for significance between the two groups ($p = 0.0001$).

associations with rs2403221 T2D SNP ($\beta = -9.422$, $p = 1.931 \times 10^{-10}$). Interestingly, *Heptadecasphing-4-enine-1-phosphate* also showed the strongest association with rs2605097 CVD SNP, with the same effect size ($\beta = -9.422$, $p = 1.931 \times 10^{-10}$) (Supplementary Table S3).

Next, the analysis was implemented to investigate the association between bacterial genera and SNPs. A total of 110 bacterial genera identified from the previous 16S rRNA analysis were included. A total of 1,921 T2D-related SNPs and 4,063 CVD-related SNPs were associated with 110 bacterial genera in the pre-surgery state. Among these associations, nine were significantly associated with T2D SNPs, and 25 were significantly associated with CVD SNPs ($FDR < 0.05$). The *Fusobacterium* genus exhibited the most significant association with rs601945 T2D SNP ($\beta = 7.884607$, $p = 1 \times 10^{-10}$). On the other hand, the *UBA1819* genus had the most significant association with rs113451833 CVD SNP ($\beta = 6.73$, $p = 1.62 \times 10^{-17}$). The longitudinal analysis of the targeted SNPs and bacterial genera identified associations between 1585 T2D-related SNPs and 3381 CVD-related SNPs in the post-surgery state with 110 bacterial genera. Nine significant associations were identified between T2D SNPs and one bacterial genus, *Intestinibacter* ($|\beta| = 7.817499$, $p = 5.18 \times 10^{-9}$) (Supplementary Table S4). Interestingly, 29 distinct CVD SNPs were also associated with the same genera, with a negative effect size ($\beta = -7.817499$, $p = 5.18 \times 10^{-9}$).

Multi-omics interaction network analysis in bariatric surgery patients

A multi-omics integration approach was employed to investigate the metabolic and molecular changes associated with bariatric surgery. Data from individual omics layers were integrated to identify pathways

a.

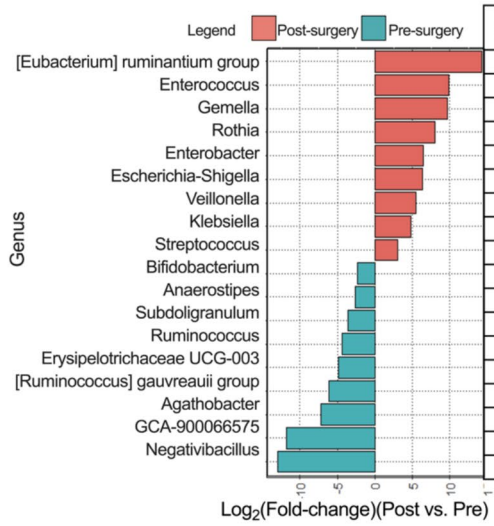

b.

	RA Pre-surgery (%)	RA Post-surgery (%)	Absolute difference	p-value	FDR q-value
[Eubacterium] ruminantium group	0.047	0.159	0.112	2.63×10^{-4}	2.90×10^{-3}
Enterococcus	0.012	1.434	1.422	9.79×10^{-6}	1.62×10^{-4}
Gemella	0.028	0.073	0.046	4.30×10^{-7}	1.06×10^{-5}
Rothia	0.033	0.083	0.050	1.43×10^{-4}	1.77×10^{-3}
Enterobacter	0.045	0.304	0.259	8.49×10^{-3}	4.67×10^{-2}
Escherichia-Shigella	0.644	5.332	4.688	2.84×10^{-6}	5.62×10^{-5}
Veillonella	0.109	1.409	1.301	3.54×10^{-7}	1.06×10^{-5}
Klebsiella	0.303	1.572	1.269	5.83×10^{-3}	3.79×10^{-2}
Streptococcus	2.056	10.931	8.875	4.22×10^{-8}	2.09×10^{-6}
Bifidobacterium	2.756	1.445	-1.311	6.51×10^{-3}	3.79×10^{-2}
Anaerostipes	1.540	1.178	-0.362	6.14×10^{-3}	3.79×10^{-2}
Subdoligranulum	2.012	0.787	-1.225	5.95×10^{-4}	5.89×10^{-3}
Ruminococcus	1.230	0.640	-0.590	1.12×10^{-3}	9.24×10^{-3}
Erysipelotrichaceae UCG-003	1.171	0.181	-0.991	1.53×10^{-3}	1.16×10^{-2}
[Ruminococcus] gauvreauii group	0.770	0.304	-0.466	2.23×10^{-5}	3.16×10^{-4}
Agathobacter	3.790	1.080	-2.710	1.18×10^{-8}	1.17×10^{-6}
GCA-900066575	0.042	0.007	-0.035	2.26×10^{-3}	1.60×10^{-2}
Negativibacillus	0.061	0.004	-0.057	8.46×10^{-4}	7.62×10^{-3}

RA: Relative abundance

c.

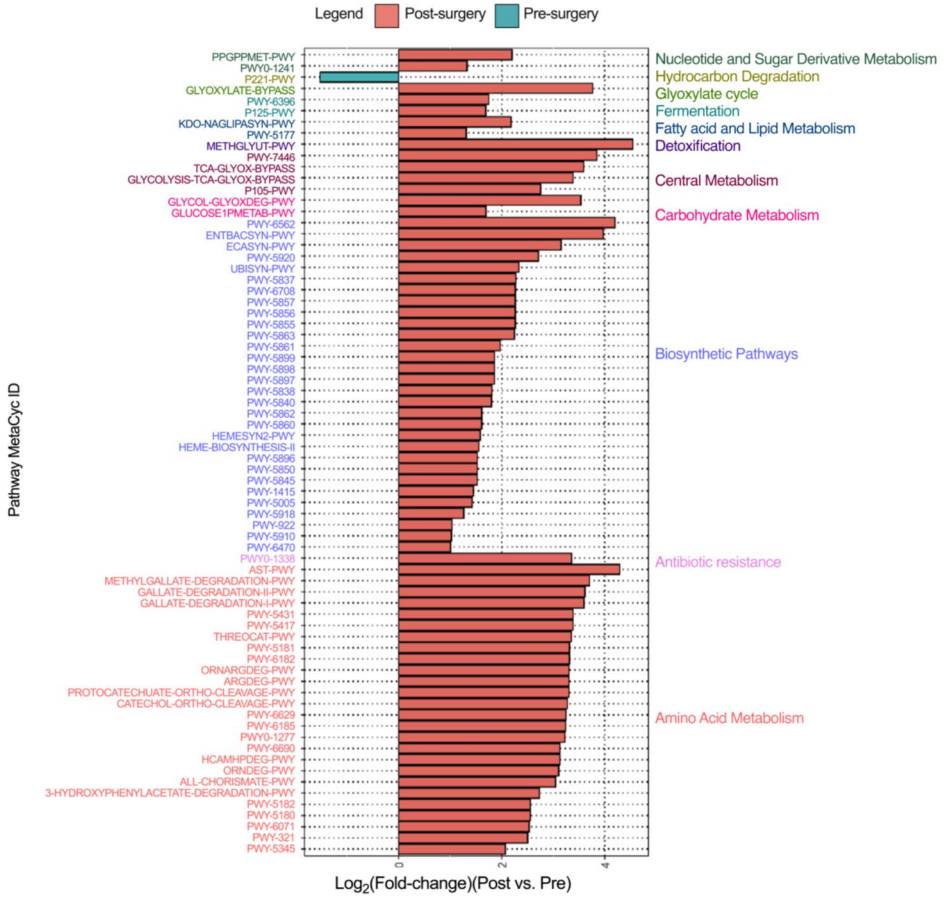

Fig. 4. Differential abundance analysis to determine the differences in the abundances of individual taxa at the genus level between pre- and post-surgery groups. (**a**) The fold-change plot shows the significant bacteria genera distinguishing between pre- and post-surgery groups. The bacteria are in descending order of their fold-change, with the most enriched in post-surgery to the most enriched before surgery. Streptococcus is the most significant bacteria genus enriched post-surgery. (**b**) The accompanying table details relative abundances, absolute differences, *p*-values, and FDR-adjusted *q*-values of the significant bacteria genus. (**c**) The functional analysis shows the 72 significantly enriched pathways that distinguish between pre- and post-surgery groups.

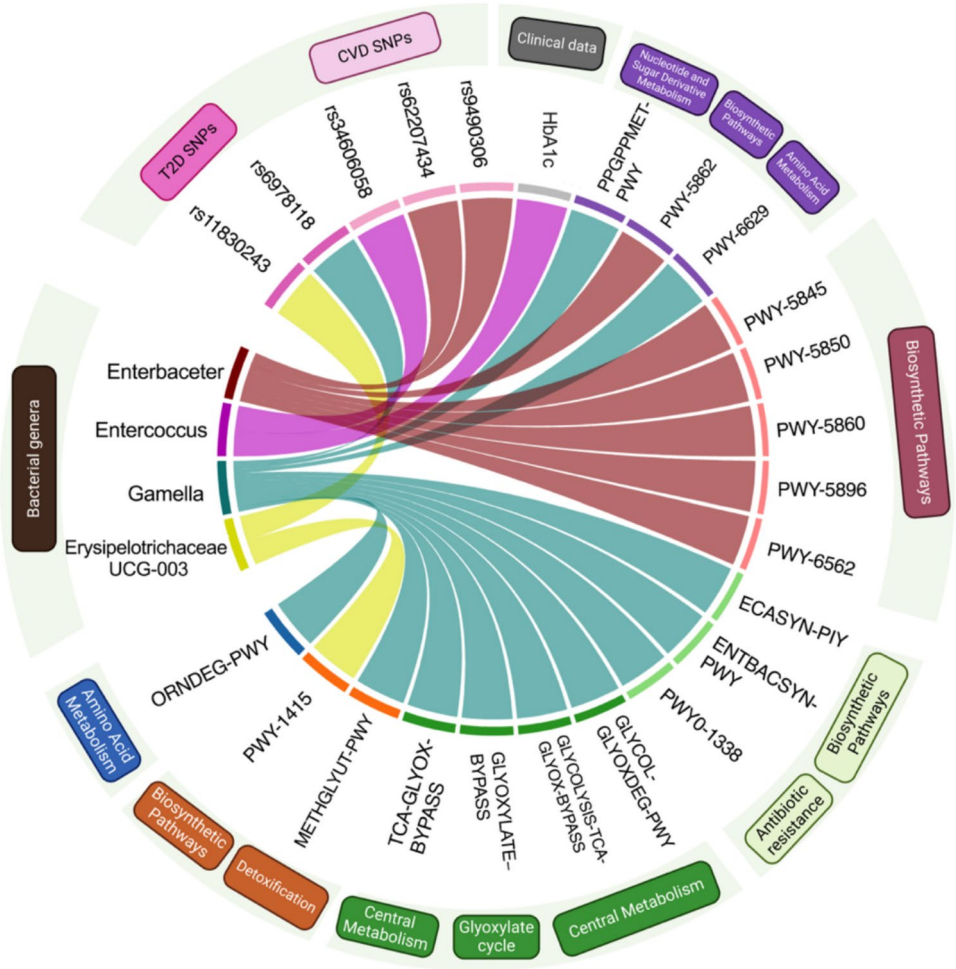

Fig. 5. Multi-omics interaction network analysis in bariatric surgery patients. Circular chord diagram illustrating key associations between host genetic variants, bacterial genera, metabolic pathways, and clinical measures. The left side of the diagram represents bacterial genera, while the right and bottom sections correspond to metabolic pathways. The upper section displays SNPs and clinical data.

and networks uniquely enriched through their combination. The multi-omics network analysis revealed a highly interconnected system linking bacterial genera, metabolites, inflammatory proteins, and clinical data, highlighting the complex interactions influenced by metabolic and molecular changes (Supplementary Fig. 10).

To expand the multi-omics network analysis, SNPs from the association analysis were incorporated to construct a more comprehensive view of host microbiome-metabolism interactions, as illustrated in Fig. 5b. The plot builds upon the metabolic pathways, clinical data, and bacterial genera from the network presented in Fig. 5a, linking them to SNPs derived from the QTL dataset. Four bacterial genera were identified for their relationship with clinical measures, genetic variants, and metabolic pathways. These genera include *Enterobacter*, *Enterococcus*, *Gemella*, and *Erysipelotrichaceae UCG-003*. The distribution of microbial abundance for each genotype is presented in Supplementary Fig. 11. Notably, *Enterococcus* and *Enterobacter* show strong links to multiple SNPs and metabolic pathways, suggesting potential genetic influence on microbial composition and metabolic functions. *Enterobacter* was linked with two CVD-associated SNPs, rs9490306 and rs62207434, and was enriched in multiple biosynthetic pathways. *Enterococcus* showed associations with the CVD SNP rs34606058 and HbA1c levels, indicating a potential role in glycemic regulation. Conversely, *Gemella* was associated with a T2D-related SNP, rs6978118, and exhibited connections to over ten metabolic pathways. These pathways belong to nucleotide and sugar derivative metabolism, amino acid metabolism, biosynthetic pathways, antibiotic resistance, detoxification, and carbohydrate and central metabolism. Lastly, *Erysipelotrichaceae UCG-003* was linked to the T2D SNP rs11830243 and one biosynthetic metabolic pathway. Overall, these findings highlight the intricate relationships between host genetics, gut microbiota, and metabolic pathways, supporting the potential role of host factors in shaping microbiome composition and function. The strong associations observed, particularly for *Enterobacter* and *Enterococcus*, underscore the need for further investigations into the genetic regulation of gut microbial dynamics and their implications for metabolic health.

Discussion

We employed a multi-omics approach to investigate the systemic effects of bariatric surgery in Emirati individuals diagnosed with diabetes or prediabetes. Patients' clinical data was analyzed to assess changes in BMI, HbA1c, lipid profile, and blood pressure before and after surgery. Our results showed significant weight loss and reductions in HbA1c, glucose levels, triglycerides, and blood pressure following bariatric surgery. These findings are consistent with previous studies highlighting the beneficial metabolic effects of bariatric surgery[29,30,31,32,33]. Sex differences in weight loss patterns were evident, with females achieving higher EBWL at 9 months, whereas males experienced greater EBWL at 3 months and maintained steady reductions throughout follow-ups. These findings are consistent with Hider et al.[34], who reported that men tend to lose more absolute weight while women show a more significant reduction in BMI following bariatric surgery. This variation is likely due to differences in body composition, as men typically experience a greater percentage of fat mass loss while increasing fat-free mass[35].

Despite evidence that weight loss improves metabolism and inflammation biomarkers, its overall impact on metabolic health remains unclear. This study examined key cardiometabolic and inflammatory proteins, revealing post-surgical improvements in several biomarkers. Anti/pro-inflammatory cytokines such as IL-1Ra, IL-4, IL-6Ra, and TNF-α showed a downward trend, with significant reductions at 9 months, aligning with previous studies on SG and RYGB[36,37]. Notably, TNF-α, known for its role in impairing glucose metabolism, decreased post-surgery. Additionally, APRIL (TNFSF13), a TNF superfamily protein, showed a significant reduction ($p = 0.0190$) at 9 months, suggesting potential immune modulation effects. Conversely, FGF-basic protein increased, likely promoting tissue repair and angiogenesis for wound healing and the formation of new blood vessels[38]. However, other inflammatory markers, including CD30, Osteopontin, GB130, and MCP-1, remained unaffected after bariatric surgery.

Through untargeted metabolomics, we identified biomarkers and pathways significantly altered by bariatric surgery. In pre-surgery samples, 25 metabolites were enriched, including *Leukotriene B4 ethanolamide*, *15-HpEPE*, *Corosolic acid*, and *Hederagenin*. *Leukotriene B4 ethanolamide* plays a role in inflammation and immune responses[39], while *15-HpEPE*, an omega-3 derivative, has anti-inflammatory properties[40]. Their involvement in obesity, T2D, or bariatric surgery remains unexplored, though their modulation may reflect increased systemic inflammation. *Corosolic acid* and *Hederagenin*, known for their anti-diabetic and anti-inflammatory effects, may have been influenced by pre-surgery supplement use[41]. Post-surgery, 73 distinct metabolites were enriched, with key metabolites such as *1-(5Z,8Z,11Z,14Z-Eicosatetraenoyl)-sn-glycero-3-phosphoethanolamine*, *cis-5,8,11-Eicosatrienoic acid*, and *Indoxyl Sulfate*. The first is involved in insulin signaling and glucose uptake[42], while *cis-5,8,11-Eicosatrienoic acid* regulates inflammatory responses[43]. *Indoxyl Sulfate*, a gut microbiota-derived metabolite, is associated with oxidative stress and CVD risk[44,45]. We identified enrichment in eight pathways, primarily involving glycerophospholipid metabolism, retinol metabolism, and folate biosynthesis. Glycerophospholipid metabolism is essential for maintaining cellular membrane integrity, lipid signaling, and membrane remodeling[46]. Retinol metabolism plays a crucial role in vitamin A processing, impacting vision, immune function, and cellular differentiation, and has been linked to diseases such as T1D, T2D, obesity, and cancer[47,48]. Folate biosynthesis supports DNA/RNA synthesis, cell proliferation, and epigenetic regulation, with a significant role in metabolic health by influencing obesity and T2D through one-carbon metabolism and DNA methylation[49,50].

We investigated features of dysbiosis using 16S rRNA sequencing and identified a higher F/B ratio in pre-surgery patients at the phylum level. An elevated F/B ratio is associated with obesity due to increased energy harvest from the diet[51]. Previous reports have shown that bariatric surgery has a key impact on reducing the F/B ratio, which aligns with the findings of this study[53–53]. These studies have also reported that improvements in inflammatory profiles accompany the decrease in the F/B ratio post-surgery. In addition, the increased relative abundance of genera such as *Akkermansia*, *Escherichia-Shigella*, and *Streptococcus* post-surgery reflects changes likely driven by altered nutrient availability, bile acid modifications, and shifts in gut pH. *Streptococcus* was the most enriched genus in post-surgery patients, which aligns with previous studies[52,54,55]. *Akkermansia* is particularly interesting since it has an inverse relationship with obesity and insulin sensitivity[54,56]. Conversely, the significant reduction in *Agathobacter*, *Bifidobacterium*, and *Faecalibacterium* highlights the complexity of potentially novel dynamics in the gut microbiome following bariatric surgery. We also explored the functional analysis of the gut microbiome, which revealed significant shifts in microbial metabolic pathways, indicating an adaptive response to the altered gastrointestinal environment. Post-surgery, an enrichment in pathways related to antibiotic resistance, biosynthesis, central metabolism, and amino acid and carbohydrate metabolism was identified, aligning with findings from previous studies[57,58].

The analysis of the association network identified four key bacterial genera (*Enterobacter, Enterococcus, Gemella,* and *Erysipelotrichaceae UCG-003*) associated with two T2D SNPs (rs11830243 and rs6978118) and three CVD SNPs (rs9490306, rs62207434, and rs34606058). These genera were the central nodes of the network, connecting host genetic variants, metabolic pathways, and clinical data, highlighting their broader role in host-microbiome interactions. These associations suggest that host genetic factors may influence microbial composition, potentially shaping metabolic functions and disease susceptibility. These results highlight the translational potential of integrating multidimensional data to better capture the complexity of biological systems and enhance precision in disease management. While adding to the knowledge of a biological system, this approach also establishes a basis for further research focused on applying these multi-omics datasets to create tailored solutions and treatment techniques.

This study provides a multi-layered perspective on the physiological changes following bariatric surgery by characterizing the relationships between clinical variables, genetic variation, protein expression, and metabolic and microbiome profiles. These insights inform future research into individualized therapeutic strategies and serve as a foundation for studies in pharmaco-omics. Continuous monitoring of HbA1c, glucose levels, lipid

profiles, and blood pressure can help refine treatment strategies and improve outcomes. Given the variability in responses, such as sex differences in weight loss patterns and lipid metabolism, precision medicine approaches incorporating metabolic, hormonal, and lifestyle factors are crucial. Pharmacogenomics labels genetic variants that affect drug metabolism and efficacy, leading to more personalized treatment strategies. Pharmacoproteomics provides an understanding of protein-level changes post-surgery, revealing biomarkers that can guide targeted therapies. Key findings include a reduction in pro/anti-inflammatory cytokines (IL-8, IL-1Ra, IL-4, IL-6Ra, TNF-α) and myocardial injury markers (hsTnI, MYO), alongside an increase in tissue repair proteins like FGF-basic.

Additionally, TNFSF13 decreased significantly post-surgery, suggesting its potential role in immune modulation and metabolic regulation, which could enhance post-surgical therapeutic strategies for metabolic disease management. Pharmacometabolomics highlights shifts in metabolic pathways that can inform drug dosing and formulation. Key metabolites involved in lipid metabolism, inflammation, and energy regulation have demonstrated the impact of bariatric surgery on the body's metabolomic profile. Metabolites like *Leukotriene B4 ethanolamide*, *15-HpEPE*, *Indoxyl Sulfate,* and *Corosolic acid* are potential pharmacometabolic biomarkers reflecting inflammation, insulin sensitivity, and oxidative stress. This understanding sheds light on how bariatric surgery can influence drug response and metabolic health, offering insights for more targeted treatments. Pharmacomicrobiomics explores the interaction between the gut microbiome and drugs. The central microbial taxa identified could influence drug response and T2D remission through their roles in metabolic pathways, inflammation, and hormonal regulation. These bacteria may modulate insulin sensitivity and inflammatory responses, affecting the efficacy of drugs like metformin and GLP-1 agonists. Such approaches hold promise for optimizing drug delivery, improving treatment outcomes, and providing a basis for long-term economic health analyses. Ultimately, these approaches can inform the development of evidence-based policies, guide future personalized medicine strategies, and shape national healthcare frameworks to promote better patient care.

Limitations

A major limitation of this study is the small sample size, which constrains the ability to detect subtle effects and reduces the extent to which findings can be generalized to broader populations. The study employs stringent and unique inclusion criteria to ensure that only suitable candidates who meet specific clinical and molecular profiles are selected. In addition, this study primarily focuses on the metabolic outcomes following bariatric surgery without comparing the effects of different surgical procedures. Although the cohort includes both individuals with type 2 diabetes (T2D) and prediabetes, outcomes were analyzed in aggregate to preserve statistical power. Subgroup analyses would be underpowered due to sample size constraints and are therefore reserved for future studies with larger cohorts, where differential responses to surgery can be more reliably evaluated. In addition, although the cohort included different bariatric procedures (SG, RYGB, GB, and SADI), stratified analyses were not feasible due to small subgroup sizes. Another inherent challenge of cohort studies is missing data, particularly the loss of samples at follow-up time points. Such missing data may reduce the power and consistency of association analysis, potentially leading to false negative or false positive relationships between SNPs and omics features. Despite these limitations, this study provides a strong foundation for understanding bariatric surgery outcomes in Emirati patients with T2D and severe obesity. Addressing these limitations in future research by increasing sample size, incorporating advanced multi-omics techniques, extending follow-up periods, and including a healthy control group will further enhance the translational significance of the findings.

Conclusion

In conclusion, by exploring multi-omics data, we showed that bariatric surgery significantly alters molecular pathways and systemic processes, contributing to improved metabolic health and diabetes remission. The integration of genomic data highlighted genetic variants linked to T2D and CVD, while proteomic analysis revealed key changes in circulating proteins linked to inflammation and CVDs. Metabolomic profiling identified metabolite shifts related to folate biosynthesis, glycerophospholipid metabolism, and retinol metabolism pathways. Gut microbiome analysis demonstrated significant changes in microbial composition and diversity, with an increase in beneficial taxa associated with improved gut health and metabolic outcomes. Finally, the association network identified four key bacterial genera (*Enterobacter*, *Enterococcus*, *Gemella*, and *Erysipelotrichaceae UCG-003*) as central nodes, showing significant associations with both genetic variants and metabolic pathways. Together, these findings provide a comprehensive multi-omics perspective on the mechanisms by which bariatric surgery drives systemic metabolic reprogramming and leads to significant health improvements in diabetic and prediabetic individuals, offering valuable insights for personalized therapeutic use in the future.

Data availability

The whole-genome and microbiome sequencing datasets generated during this study have been deposited in the European Nucleotide Archive (ENA) at the European Bioinformatics Institute (EBI) under accession number PRJEB88699. All other data generated or analyzed during this study are available within the published article and its Supplementary Information files.

Received: 8 April 2025; Accepted: 1 August 2025
Published online: 09 August 2025

References

1. *International Textbook of Diabetes Mellitus*. (Wiley, 2015). https://doi.org/10.1002/9781118387658.

2. *IDF Diabetes Atlas Eighth Edition*. http://dx.doi. org/https://doi.org/10.1016/S0140-6736(16)31679-8. (2017).
3. Home *et al.* IDF Diabetes Atlas 2021 | IDF Diabetes Atlas. https://diabetesatlas.org/atlas/tenth-edition/ (2021).
4. Alkharaiji, M., Anyanwagu, U., Donnelly, R. & Idris, I. Effect of bariatric surgery on cardiovascular events and metabolic outcomes in obese patients with insulin-treated type 2 diabetes: a retrospective cohort study. *Obes. Surg.* **29**, 3154–3164 (2019).
5. Aakre, K. M. et al. Gastric bypass surgery is associated with reduced subclinical myocardial injury and greater activation of the cardiac natriuretic peptide system than lifestyle intervention. *Clin. Biochem.* **86**, 36–44 (2020).
6. El-Zawawy, H. T., El-Aghoury, A. A., Katri, K. M., El-Sharkawy, E. M. & Gad, S. M. S. Cortisol/DHEA ratio in morbidly obese patients before and after bariatric surgery: Relation to metabolic parameters and cardiovascular performance. *Int. J. Obes.* **46**, 381–392 (2022).
7. Lautenbach, A. et al. Long-term improvement of chronic low-grade inflammation after bariatric surgery. *Obes. Surg.* **31**, 2913–2920 (2021).
8. Almby, K. E. et al. Time course of metabolic, neuroendocrine, and adipose effects during 2 years of follow-up after gastric bypass in patients with type 2 diabetes. *J. Clin. Endocrinol. Metab.* **106**, e4049–e4061 (2021).
9. Härma, M.-A. et al. Gastrointestinal manifestations after Roux-en-Y gastric bypass surgery in individuals with and without type 2 diabetes. *Surg. Obes. Relat. Dis.* **17**, 585–594 (2021).
10. Zhao, S. et al. Short-term metabolic changes and their physiological mediators in the Roux-en-Y gastric bypass bariatric surgery. *Obes. Surg.* **34**, 625–634 (2024).
11. Lau, E. et al. Gut microbiota changes after metabolic surgery in adult diabetic patients with mild obesity: a randomised controlled trial. *Diabetol. Metab. Syndr.* **13**, 1–15 (2021).
12. Benton, M. C. et al. An analysis of DNA methylation in human adipose tissue reveals differential modification of obesity genes before and after gastric bypass and weight loss. *Genome Biol.* **16**, 8 (2015).
13. Vohl, M.-C. Differential methylation of inflammatory and insulinotropic genes after metabolic surgery in women. *J. Clin. Epigen.* **1**, 1–9 (2015).
14. Kopanos, C. et al. VarSome: the human genomic variant search engine. *Bioinformatics* **35**, 1978–1980 (2019).
15. Pang, Z. et al. Using MetaboAnalyst 5.0 for LC–HRMS spectra processing, multi-omics integration and covariate adjustment of global metabolomics data. *Nat. Protoc.* **17**, 1735–1761 (2022).
16. Love, M. I., Huber, W. & Anders, S. Moderated estimation of fold change and dispersion for RNA-seq data with DESeq2. *Genome Biol.* **15**, 550 (2014).
17. Lê, S., Josse, J. & Husson, F. FactoMineR: An R package for multivariate analysis. *J. Stat. Softw.* **25**, 1–18 (2008).
18. Kassambara, A. & Mundt, F. *factoextra: Extract and Visualize the Results of Multivariate Data Analyses* (The R Foundation, 2020).
19. Zhang, B., Kirov, S. & Snoddy, J. WebGestalt: an integrated system for exploring gene sets in various biological contexts. *Nucleic Acids Res.* **33**, W741–W748 (2005).
20. Callahan, B. J. et al. DADA2: High-resolution sample inference from Illumina amplicon data. *Nat. Methods* **13**, 581–583 (2016).
21. McMurdie, P. J. & Holmes, S. phyloseq: An R package for reproducible interactive analysis and graphics of microbiome census data. *PLoS ONE* **8**, e61217 (2013).
22. Shabalin, A. A. Matrix eQTL: ultra fast eQTL analysis via large matrix operations. *Bioinformatics* **28**, 1353–1358 (2012).
23. Benjamini, Y. & Hochberg, Y. Controlling the false discovery rate: A practical and powerful approach to multiple testing. *J. Royal Stat. Soc. Ser. B (Methodol.)* **57**, 289–300 (1995).
24. van Buuren, S. & Groothuis-Oudshoorn, K. Mice: Multivariate imputation by chained equations in R. *J. Stat. Soft.* **45**, 1–67 (2011).
25. Ritchie, M. E. et al. limma powers differential expression analyses for RNA-sequencing and microarray studies. *Nucleic Acids Res.* **43**, e47 (2015).
26. Csárdi, G. et al. igraph for R: R interface of the igraph library for graph theory and network analysis. Zenodo https://doi.org/10.5281/zenodo.10681749 (2024).
27. Gu, Z., Gu, L., Eils, R., Schlesner, M. & Brors, B. circlize implements and enhances circular visualization in R. *Bioinformatics* **30**, 2811–2812 (2014).
28. Kanehisa, M. & Goto, S. KEGG: kyoto encyclopedia of genes and genomes. *Nucleic Acids Res.* **28**, 27–30 (2000).
29. Castro, M.-J. et al. Long-term weight loss results, remission of comorbidities and nutritional deficiencies of sleeve gastrectomy (SG), Roux-En-Y gastric bypass (RYGB) and one-anastomosis gastric bypass (OAGB) on type 2 diabetic (T2D) patients. *Int. J. Environ. Res. Public Health* **17**, 7644 (2020).
30. Coleman, K. J. et al. Comparative safety and effectiveness of Roux-en-Y gastric bypass and sleeve gastrectomy for weight loss and type 2 diabetes across race and ethnicity in the PCORnet bariatric study cohort. *JAMA Surg.* **157**, 897–906 (2022).
31. Dewberry, L. C. et al. Weight loss and health status 5 years after adjustable gastric banding in adolescents. *Obes. Surg.* **30**, 2388–2394 (2020).
32. Khan, K. et al. Improvement in glycated hemoglobin A1C after laparoscopic Roux-en-Y gastric bypass and sleeve gastrectomy in an ethnically diverse population with diabetes. *Surg. Obes. Relat. Dis.* **16**, 1414–1418 (2020).
33. Wachsmann, A. et al. Impact of pre-operative glycated haemoglobin A1C level on 1-year outcomes of endovascular treatment in patients with critical limb ischemia in the course of diabetes mellitus. *Folia Med. Cracov.* **59**, 49–60 (2019).
34. Hider, A. M. et al. Association of sex differences on weight loss and complications following bariatric surgery. *J. Surg. Res.* **299**, 359–365 (2024).
35. Hassan Zadeh, M. et al. Changes in fat mass index and fat-free mass index vary significantly by age and sex of the patient, and by type of bariatric surgery. *Obes. Surg.* **34**, 3781–3789 (2024).
36. Katsogiannos, P. et al. Changes in circulating cytokines and adipokines after RYGB in patients with and without type 2 diabetes. *Obesity* **29**, 535–542 (2021).
37. Subramaniam, R. et al. Sleeve gastrectomy and Roux-en-Y gastric bypass attenuate pro-inflammatory small intestinal cytokine signatures. *Obes. Surg.* **29**, 3824–3832 (2019).
38. Farooq, M., Khan, A. W., Kim, M. S. & Choi, S. The role of fibroblast growth factor (FGF) signaling in tissue repair and regeneration. *Cells* **10**, 3242 (2021).
39. McHugh, D. et al. Novel compounds that interact with both leukotriene B4 receptors and vanilloid TRPV1 receptors. *J. Pharmacol. Exp. Ther.* **316**, 955–965 (2006).
40. Maskrey, B. H., Megson, I. L., Rossi, A. G. & Whitfield, P. D. Emerging importance of omega-3 fatty acids in the innate immune response: Molecular mechanisms and lipidomic strategies for their analysis. *Mol. Nutr. Food Res.* **57**, 1390–1400 (2013).
41. Cannarella, R., Garofalo, V. & Calogero, A. E. Anti-dyslipidemic and anti-diabetic properties of corosolic acid: A narrative review. *Endocrines* **4**, 616–629 (2023).
42. Tsuchiya, A., Kanno, T. & Nishizaki, T. Dipalmitoleoylphosphoethanolamine as a PP2A enhancer obstructs insulin signaling by promoting Ser/Thr dephosphorylation of Akt. *Cell. Physiol. Biochem.* **34**, 617–627 (2014).
43. Owen, W. F. Cytokine regulation of eicosanoid synthesis. *Lipid Mediat. Allergic Dis. Respir. Tract* https://doi.org/10.1201/9781003574507-9 (2024).
44. Ribeiro, A. et al. Uremic toxin indoxyl sulfate promotes macrophage-associated low-grade inflammation and epithelial cell senescence. *Int. J. Mol. Sci.* **24**, 8031 (2023).
45. Takkavatakarn, K. et al. Association between indoxyl sulfate and dialysis initiation and cardiac outcomes in chronic kidney disease patients. *Int. J. Nephrol. Renov. Dis.* **15**, 115–126 (2022).

46. Zan, X. et al. Glycerophospholipids. In *Fungal Lipid Biochemistry* (ed. Zan, X.) (Bentham Science Publishers, 2023). https://doi.org/10.2174/9789815123012123010010.
47. Ross, A. C. Vitamin A: Physiology, dietary sources and requirements. In *Encyclopedia of Human Nutrition* (ed. Ross, A. C.) (Elsevier, 2023).
48. Han, H. et al. Retinol metabolism signaling participates in microbiota-regulated fat deposition in obese mice. *J. Nutr. Biochem.* **136**, 109787 (2025).
49. Zheng, Y. & Cantley, L. C. Toward a better understanding of folate metabolism in health and disease. *J. Exp. Med.* **216**, 253–266 (2019).
50. Zhao, P. et al. Adaptation of intestinal and bile acid physiology accompany the metabolic benefits following ileal interposition in the rat. *Obes. Surg.* **28**, 725–734 (2018).
51. Hirata, B. K. S. et al. Ginkgo biloba extract (GbE) restores gut microbiota dysbiosis in a rat model of lard-rich diet-induced obesity. *Phytomed. Plus* **3**, 100467 (2023).
52. Al Assal, K. et al. Gut microbiota profile of obese diabetic women submitted to Roux-en-Y gastric bypass and its association with food intake and postoperative diabetes remission. *Nutrients* **12**, 278 (2020).
53. Magne, F. et al. The firmicutes/bacteroidetes ratio: A relevant marker of gut dysbiosis in obese patients?. *Nutrients* **12**, 1474 (2020).
54. Aron-Wisnewsky, J. et al. Major microbiota dysbiosis in severe obesity: fate after bariatric surgery. *Gut* **68**, 70–82 (2019).
55. Guo, Y. et al. Modulation of the gut microbiome: a systematic review of the effect of bariatric surgery. *Eur. J. Endocrinol.* **178**, 43–56 (2018).
56. Kobyliak, N. et al. Akkermansia muciniphila as a novel powerful bacterial player in the treatment of metabolic disorders. *Minerva. Endocrinol. (Torino)* **47**, 242–252 (2022).
57. Gutiérrez-Repiso, C., Moreno-Indias, I. & Tinahones, F. J. Shifts in gut microbiota and their metabolites induced by bariatric surgery. Impact of factors shaping gut microbiota on bariatric surgery outcomes. *Rev. Endocr. Metab. Disord.* **22**, 1137–1156 (2021).
58. Shen, N. et al. Longitudinal changes of microbiome composition and microbial metabolomics after surgical weight loss in individuals with obesity. *Surg. Obes. Relat. Dis.* **15**, 1367–1373 (2019).

Acknowledgements

We would like to acknowledge Ms. Khayce Juma for her valuable assistance with sample collection and registration.

Author contributions

BA: Writing—original draft & data analysis. MM: Writing—review & editing. AB: Data analysis. SR: Sequencing & data analysis. SPS: Sequencing & data analysis. SKA: Writing—review & editing. SE: Writing—review & editing. NM: Data analysis. MO: Writing—review & editing. J.S.B.-G: Writing—review & editing. C.A: Writing—review & editing. JR: Writing—review & editing. JPP: Writing—review & editing. JR: Writing—review & editing. GDDG: Writing—review & editing. MA: Writing—review & editing. MAB: Data analysis. SSA: Data analysis. H.A: Supervision– review & editing.

Funding

This work was supported by The Abu Dhabi Department of Education and Knowledge (ADEK) (grant number 8434000344).

Declarations

Competing interests

The authors declare no competing interests.

Additional information

Supplementary Information The online version contains supplementary material available at https://doi.org/10.1038/s41598-025-14577-w.

Correspondence and requests for materials should be addressed to H.A.S.